

Received 30 November 2023, accepted 15 December 2023, date of publication 19 December 2023,
date of current version 26 December 2023.

Digital Object Identifier 10.1109/ACCESS.2023.3344839

RESEARCH ARTICLE

Investigation of Noise Sources in Fractional-Slot Concentrated Winding Motors Considering High-Order Radial/Tangential Electromagnetic Force Combination and Modulation

XIXIN RAO¹, LV RONG¹, WUSHENG GAN¹, CHENGDI XIAO^{1,2}, AND YI ZHOU²

¹School of Advanced Manufacturing, Nanchang University, Nanchang 330031, China

²Research and Development Center, Shanghai Highly Electric Company Ltd., Shanghai 201206, China

Corresponding author: Chengdi Xiao (422414067@qq.com)

This work was supported by the “Revealing the List and Appointing Leaders” Project under the Major Scientific and Technological Research and Development Special Program of Jiangxi Province under Grant 20223AAE02012.

ABSTRACT Traditional methods equate the slotted stator as an unslotted model and employ an approximation where the stator deformations are considered inversely proportional to the fourth power of the order of air-gap electromagnetic force density (AEFD). This approach effectively overlooks the contributions of high-order forces. Furthermore, it overlooks the influence of tangential forces, as radial forces typically have significantly greater amplitudes than tangential. However, the effectiveness of this method has been questioned. This study aims to establish a novel method for accurately identifying the harmonic components of AEFD responsible for vibration noise by investigating the electromagnetic vibration noise source in a 9-slot/6-pole fractional-slot concentrated-winding interior permanent magnet synchronous machine (FSCW-IPMSM). Initially, the modulation law of high-order force waves is investigated through a force conversion model, revealing the mechanism behind the strong modulation effect of high-order force waves. Subsequently, a quantitative analysis modulation force model is proposed. Building on this foundation, a multi-physics field coupling simulation method is employed to predict the electromagnetic vibration noise influence mechanism of high-order radial and tangential AEFD, as well as their coupling effects. The results demonstrate that the vibration noise at the frequency of $18f_e$ in this motor is primarily induced by the coupling effects of high-order radial and tangential AEFD components. Neglecting the contribution of tangential AEFD significantly underestimates the actual vibration levels in the motor. The research outcomes emphasize the importance of considering tangential AEFD and high-order force modulation effects, providing a fresh perspective for accurately predicting the electromagnetic vibration sources in FSCW-IPMSM.

INDEX TERMS Fractional-slot concentrated-winding machine, high-order electromagnetic force, radial and tangential force, force modulation effect, motor noise source identification.

I. INTRODUCTION

As air conditioners become more widespread, the demand for living comfort continues to rise, and the accompanying vibration issues in air conditioning systems are increasingly recognized. The noise level of household air conditioners

The associate editor coordinating the review of this manuscript and approving it for publication was Xiaodong Liang.

has emerged as a crucial reference indicator for consumers when purchasing these appliances. The compressor, one of the primary sources of noise in air conditioners, generates electro-magnetic vibration and noise during operation, which not only reduces user comfort but also constrains the development of air conditioning sound quality. Consequently, it is essential to quantitatively evaluate and reduce vibration and noise at the compressor design stage to meet low noise

requirements. Fractional slot concentrated winding (FSCW) motors, known for their compact structure, high torque density, and high efficiency [1], have been extensively employed in applications such as variable-frequency air-conditioning compressors. However, the use of FSCW results in stator magnetic potential rich in harmonics [2], [3]. Through the force modulation effect, high-order force waves are modulated into low-order force waves by the stator teeth [4], exacerbating motor vibration.

Numerous studies have focused on predicting motor vibration and noise. In the early 1920s, Fritze first proposed that electromagnetic vibration is generated by the interaction of radial air-gap electromagnetic forces (AEFD) between the stator and rotor [5]. In the investigation of vibration and noise issues in FSCW motors, various researchers have explored the electro-magnetic vibration of FSCW motors with different pole-slot combinations, the impact of radial and tangential modulation force effects on vibration, and the role of tangential forces in reducing or enhancing vibrations caused by radial forces in different scenarios. Islam et al. [6] investigated the electromagnetic vibration of FSCW-IPMSM with different pole-slot combinations through finite element analysis (FEA) and found that low torque pulsation cannot guarantee low vibration and noise of the motor. The low-order modal vibration caused by low-order forces is the main source of motor vibration and noise. Jordan [7] equated the motor stator to a toothless model and found that the vibration deformation of permanent magnet (PM) motors is inversely proportional to the fourth power of the radial force space order. Subsequent scholars generally believed that the lowest-order radial force plays a dominant role in the vibration performance of FSCW motors [8], [9], [10], [11], [12], [13], and the contribution of high-order electromagnetic force harmonic components is usually ignored.

As research into electromagnetic forces progresses, Fang et al. [14] introduced a concentrated force conversion model to equate the AEFD to concentrated force and torque. In accordance with the sampling theorem, they revealed that the stator's tooth-slot structure modulates high-order force waves. Subsequently, a comparative analysis of the vibrations of two different motors indirectly confirmed that the modulation effect of the stator's teeth on high-order force waves induces significant low-order modal vibrations within the motor. This indicates that accounting for the modulation effect of stator teeth on high-order force waves can enhance the accuracy of motor vibration analysis. To address the impact of modulation effects on vibration, Fang et al. [15] introduced a hybrid analysis model that combines finite element (FE) and experimental methods. By obtaining the structural response transfer function through hammering and computing the vibration response using modal superposition, it was revealed that neglecting the contribution of high-order force waves would result in substantial deviations in predicted vibration. Kim et al. [16] compared two FSCW motors with different slot-pole numbers and analyzed the

influence of variations in radial and tangential modulation force effects on vibration. The findings indicated that larger modulation forces are more detrimental to vibration, and tangential force effects also play a significant role in affecting vibration. Liang et al. [17] proposed a model to examine the electromagnetic force modulation effect by equivalently applying the AEFD to the stator yoke. The study showed that high-order force waves, under the influence of teeth, generate low-order modulation vibrations, and the amplitude of modulation vibrations is solely related to the stator slot opening. Zhao et al. [18] discovered that motor vibrations under low-speed and heavy-load conditions are primarily attributed to electro-magnetic force modulation and stator magnetomotive force (MMF) harmonics. Yin et al. [19] through a force conversion model quantitatively analyzed the contribution of radial modulation force to air-gap flux density (AFD) amplitude and modulation coefficient under no-load motor conditions but did not consider the contribution of tangential AEFD to vibration and the contribution of different harmonic orders of AEFD to modulation force. Furthermore, some researchers have studied tangential forces [20], [21] and found that tangential forces, as an objective local force, can either reduce or amplify vibrations caused by radial forces in different scenarios. The studies mentioned above indicate that the previous methods for analyzing motor vibrations have limitations because high-order electromagnetic force harmonics induce low-order modal deformations in the motor due to the modulation effect of the stator's slot structure on high-order electromagnetic force waves. For fractional slot concentrated windings suffering from vibration noise issues, due to the presence of numerous harmonic components in the air-gap electromagnetic force, the analysis of motor vibrations cannot be limited to considering only the contribution of low-order radial electromagnetic forces to vibration noise, as in previous research. This is because high-order electromagnetic forces induce low-order modal vibrations in the motor under the force modulation effect. Additionally, tangential electromagnetic forces can also impact motor vibrations, and neglecting their contribution may lead to inaccuracies in vibration analysis. However, there is currently a lack of comprehensive research on the impact of these factors on motor vibrations and precise methods for identifying the key harmonic components of electromagnetic forces responsible for inducing motor vibrations. This is because the air-gap electromagnetic force contains numerous harmonic components, and high-order force harmonics exhibit force modulation phenomena. Both radial and tangential forces contribute to motor vibrations, with the contribution of tangential electromagnetic forces being non-negligible. This presents a challenge in accurately identifying the critical two-dimensional harmonic components of electromagnetic forces responsible for motor vibrations.

Numerous studies have delved into the impact of radial and tangential electromagnetic forces on vibration, revealing that higher-order electromagnetic force harmonics can

instigate low-order modal phenomena in the stator, a process modulated by stator teeth. While these studies have primarily been conducted in the context of electric vehicles and industrial control motors, they provide valuable insights for mitigating electromagnetic vibration noise in permanent magnet (PM) synchronous motors used in compressors. However, current research on motor vibration sources does not concurrently consider the effect of high-order force wave modulation and the coupling effects of radial and tangential AEFD on vibration noise. Consequently, accurately discerning the differences in motor vibration noise induced by various AEFD harmonic components remains a formidable challenge. Variable-frequency air conditioning compressor FSCW-IPMSM possess unique characteristics and requirements, such as a broad speed regulation range, compact size and weight, and a heightened sensitivity to vibration noise. Despite these distinct attributes, research specifically addressing motor noise and vibration in the context of variable-frequency air conditioning remains limited. The electromagnetic vibration noise generated by compressor motors is a result of harmonic electromagnetic forces within the air gap. Hence, accurately pinpointing the source of this electromagnetic vibration noise is essential for efficiently mitigating electromagnetic noise. Moreover, the ability to identify specific pivotal two-dimensional harmonic components of electromagnetic forces responsible for the noise prior to optimizing motor vibration noise can eliminate the necessity for additional multiphysics field coupling simulations. This streamlined approach substantially enhances the efficiency of vibration noise optimization while still achieving favorable optimization outcomes.

To accurately identify the AEFD harmonic components that cause vibration noise in FSCW-IPMSM while considering the contribution of high-order force modulation effects and tangential AEFD, the electromagnetic noise mechanism of a 9-slot/6-pole FSCW-IPMSM for variable-frequency air conditioning compressors is conducted in this paper. Firstly, the AEFD is calculated, and the mechanism of stator teeth modulating high-order radial and tangential AEFD waves through a concentrated force model is analyzed. Then, a decoupling model for quantitatively analyzing modulation forces is proposed to assess the contribution of different spatial order electromagnetic force harmonics to modulation forces. Finally, to accurately predict the electromagnetic vibration response of the motor, the motor stator is modeled as an anisotropic material. The stator FE model is calibrated by modal experiments using the hammering method. Through multi-physics field coupling simulation, the contributions of radial and tangential force waves are considered separately to predict the vibration noise of the compressor motor.

II. ELECTROMAGNETIC VIBRATION SOURCE

With the deepening of research on AEFD, the contribution of high-order force waves to vibration has gradually been valued. Existing research shows that high-order force waves can also produce low-order vibrations, which are called mod-

ulation vibrations. The difference from traditional motors is that the modulation vibration of FSCW-IPMSM is more obvious. The previous conclusion that the influence of high-order force waves on vibration is ignored is no longer applicable. At the same time, the influence of tangential forces on motor vibration has been given due attention. Considering the contribution of tangential forces will aid in improving the accuracy of motor vibration analysis.

Therefore, it is of great significance to accurately identify the main electromagnetic vibration source before optimizing vibration noise. The object of this study is a FSCW-IPMSM for air conditioning compressor. Fig. 1 shows the schematic diagram of the motor and its main parameters are shown in Table 1.

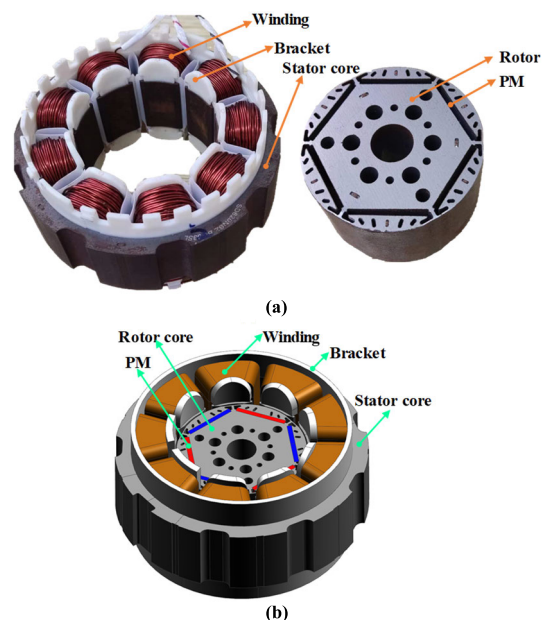


FIGURE 1. Motor diagram. (a) Physical drawings. (b) Equivalent model drawings.

TABLE 1. Main parameters of FSCW-IPMSM.

Items (Unit)	Value
Number of slots/poles	9/6
Air-gap length (mm)	0.5
Rotation speed (r/min)	3000
Outer radius of stator (mm)	105
Inner radius of stator (mm)	56
Stack length of stator (mm)	30
Thickness of PM (mm)	2
Length of PM (mm)	20

This paper comprehensively addresses the impact of high-order harmonic forces and tangential/radial forces on motor vibration, identifying key two-dimensional harmonic force components. Fig. 2 presents the overall control framework of this study, The research is primarily divided into four sections: analysis of AEFD harmonics, conversion of concentrated forces equivalent (ECF) to AEFD harmonics,

calibration of the finite element model (FEM) of the motor, and determination of key two-dimensional AEFD harmonics influencing the dominant motor vibration noise.

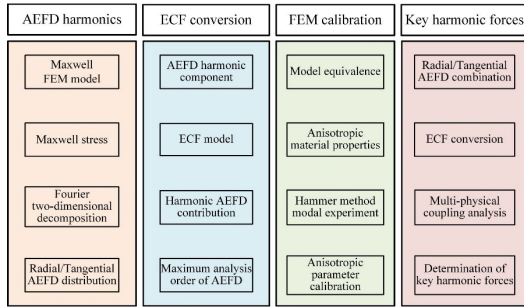


FIGURE 2. The overall control block diagram for the research content.

A. AIR-GAP FLUX DENSITY

To consider the slotting effect of stator teeth, the relative permeance function is introduced [22]:

$$\lambda(\theta) = \Lambda_0 + \sum_{k=1,2,3}^{\infty} \Lambda_k \cos(kZ_1\theta) \quad (1)$$

where Λ_0 is the amplitude of the average permeance, Λ_k is the amplitude of the k -th harmonic permeance, k is set of integers, Z_1 is slot number of stator.

When the magnetic saturation and leakage of the stator iron core are disregarded, the AFD can be calculated by multiplying the MMF based on the relative permeance function [23]. The AFD of the stator slotting model under no-load is as follow [24], [25]:

$$b_{rotor}(\theta, t) = \sum_{\mu} B_{\mu} \cos(\mu\omega t - \mu p\theta) + \sum_{\mu} \sum_{k=1}^{\infty} \frac{1}{2} B_{\mu k} \cos(\mu\omega t - (\mu p \pm kZ_1)\theta) \quad (2)$$

where $B_{\mu} = F_{\mu}\Lambda_0$ is the harmonic amplitude caused by average permeance, $B_{\mu k} = F_{\mu}\Lambda_k$ is the harmonic amplitude caused by the k -th harmonic permeance, F_{μ} is the amplitude of the μ -th harmonic of PM MMF, ω , p , θ , and t represent mechanical angular velocity of rotor, pole-pair, mechanical angle, time, respectively. $\mu = 2r_1 + 1$, $r_1 = 0, 1, 2, 3 \dots$, μ is the spatial harmonic order of the PM field.

For FSCW motors, the slot number per phase per pole q is a fraction, the stator harmonic order v is determined according to the pole/slot combination, which can be expressed as follows [16]:

$$q = \frac{Z_1}{2mp} = \frac{b}{c}, v = \frac{6r_2}{c} + 1 \quad (3)$$

where b and c are relatively prime, $r_2 = 0, \pm 1, \pm 2, \pm 3, \dots$, the positive and negative of v represents the rotation direction of the synthetic MMF.

The AFD generated by a three-phase symmetric sinusoidal current in the stator winding under load [26]:

$$b_{stator}(\theta, t) = \sum_v B_v \cos(\omega t - vp\theta + \varphi_v) + \sum_v \sum_{k=1}^{\infty} \frac{1}{2} B_{vk} \cos(\omega t - (vp \pm kZ_1)\theta + \varphi_v) \quad (4)$$

where $v = 3r_2 + 1$, $r_2 = 0, \pm 1, \pm 2, \pm 3, \dots$, $B_v = F_v\Lambda_0$ is the stator AFD harmonic amplitude caused by average permeance, $B_{vk} = F_v\Lambda_k$ is the stator AFD harmonic amplitude caused by the k -th harmonic permeance, F_v is the amplitude of the v -th harmonic of MMF, φ_v is phase of MMF, harmonics v is spatial harmonic order of the armature reaction.

When the core magnetic saturation is ignored, the AFD under the motor load is superimposed by the AFD generated by the stator armature winding and the rotor PM [27]:

$$b_r(\theta, t) = b_{rotor}(\theta, t) + b_{stator}(\theta, t) \quad (5)$$

B. AIR-GAP ELECTROMAGNETIC FORCE DENSITY

The air-gap electromagnetic force density can be solved by the Maxwell stress equation [28]:

$$p_r(\theta, t) = \frac{1}{2\mu_0} (b_r^2 - b_t^2) \\ p_{\tau}(\theta, t) = \frac{1}{\mu_0} b_r b_{\tau} \quad (6)$$

The radial component of the AFD is much larger than the tangential component. To simplify the calculation of the radial AEFD, the influence of the tangential AFD component is ignored [29]. The approximate radial AEFD in the air-gap is as follow:

$$p_r(\theta, t) = \frac{1}{2\mu_0} (b_r^2 - b_t^2) \approx \frac{1}{2\mu_0} b_r^2 = \frac{1}{2\mu_0} \{b_{rotor}^2 + b_{stator}^2 + 2b_{rotor}b_{stator}\} \quad (7)$$

According to (7), the radial AEFD wave is a result of the interaction between two AFD harmonics or their self-actions. It contains three components: the self-action of the AFD generated by the rotor, the self-action of the AFD generated by the stator, and the interaction between the AFD generated by the rotor and stator. The corresponding electromagnetic force harmonic components.

Table 2 depict three types of radial AEFD generated by different AFD. The sources of these electromagnetic forces involve not only the self or mutual interaction of different AFD, but also numerous spatial order types that are not conducive to analysis. Given that the radial electromagnetic force wave is a two-dimensional function of time and space, it can be expressed by a two-dimensional Fourier series:

$$p_r(\theta, t) = \sum_n \sum_{f_n} \sigma_{n,f_n}^r \cos(2\pi f_n t - n\theta + \varphi_n, f_n) \quad (8)$$

where σ_{n,f_n}^r represent the amplitude of the radial AEFD harmonics with spatial n order and frequency f_n .

TABLE 2. The radial AEFD harmonic.

Source	Amplitude	Spatial order	Frequency order
Rotor	$\frac{1}{4\mu_0}(B_r\Lambda_0)^2$	$2\mu p$	2μ
	$\frac{1}{2\mu_0}B_{\mu_1}B_{\mu_2}\Lambda_0^2$	$(\mu_1 \pm \mu_2)p$	$(\mu_1 \pm \mu_2)$
	$\frac{1}{16\mu_0}(B_r\Lambda_k)^2$	$2(\mu p \pm kZ_1)$	2μ
	$\frac{1}{8\mu_0}B_{\mu_1}B_{\mu_2}\Lambda_{k_1}\Lambda_{k_2}$	$(\mu_1 \pm \mu_2)p \pm (k_1 \pm k_2)Z_1$	$(\mu_1 \pm \mu_2)$
	$\frac{1}{4\mu_0}B_{\mu_1}B_{\mu_2}\Lambda_0\Lambda_k$	$(\mu_1 \pm \mu_2)p \pm kZ_1$	$(\mu_1 \pm \mu_2)$
Stator	$\frac{1}{4\mu_0}(B_v\Lambda_0)^2$	$2vp$	
	$\frac{1}{2\mu_0}B_{v_1}B_{v_2}\Lambda_0^2$	$(v_1 + v_2)p$	
	$\frac{1}{16\mu_0}(B_v\Lambda_k)^2$	$2(vp \pm kZ_1)$	2
	$\frac{1}{8\mu_0}B_{v_1}B_{v_2}\Lambda_{k_1}\Lambda_{k_2}$	$(v_1 + v_2)p \pm (k_1 \pm k_2)Z_1$	
	$\frac{1}{4\mu_0}B_{v_1}B_{v_2}\Lambda_0\Lambda_k$	$(v_1 + v_2)p \pm kZ_1$	
Rotor & Stator	$\frac{1}{2\mu_0}B_\mu B_v \Lambda_0^2$	$(\mu \pm v)p$	
	$\frac{1}{2\mu_0}B_\mu B_v \Lambda_0 \Lambda_k$	$(\mu \pm v)p \pm kZ_1$	$(\mu \pm 1)$
	$\frac{1}{8\mu_0}B_\mu B_v \Lambda_{k_1} \Lambda_{k_2}$	$(\mu \pm v)p \pm (k_1 \pm k_2)Z_1$	

From equations (6) and (7), it can be observed that both the radial and tangential AEFD are generated by the interaction of harmonics in the AFD. The radial AEFD can be approximated as originating from the self-interaction of the radial AFD, whereas the tangential AEFD is generated by the interaction between the radial and tangential AFD.

Moreover, the radial and tangential AFD maintain a constant phase difference of 90 degrees in space, leading to a harmonic distribution similarity between the radial and tangential AEFD. This observation is further supported by Fig. 3 and has also been confirmed in previous studies [15], [18]. Hence, the similarity in harmonic distribution of radial and tangential AEFD will lead to analogous motor vibration characteristics induced by both forces.

C. TOOTH CONCENTRATED FORCE

The AEFD wave acting on the stator tooth surface is distributed in the form of nodal force, as shown in (8). It can be represented as the action of a concentrated force and torque on the stator tooth [30], as depicted in Fig.4.

The concentrated force acting on the stator tooth can be decomposed into the radial and tangential equivalent concentrated force (ECF) components acting together on the tooth [30]. The radial and tangential components of the equiv-

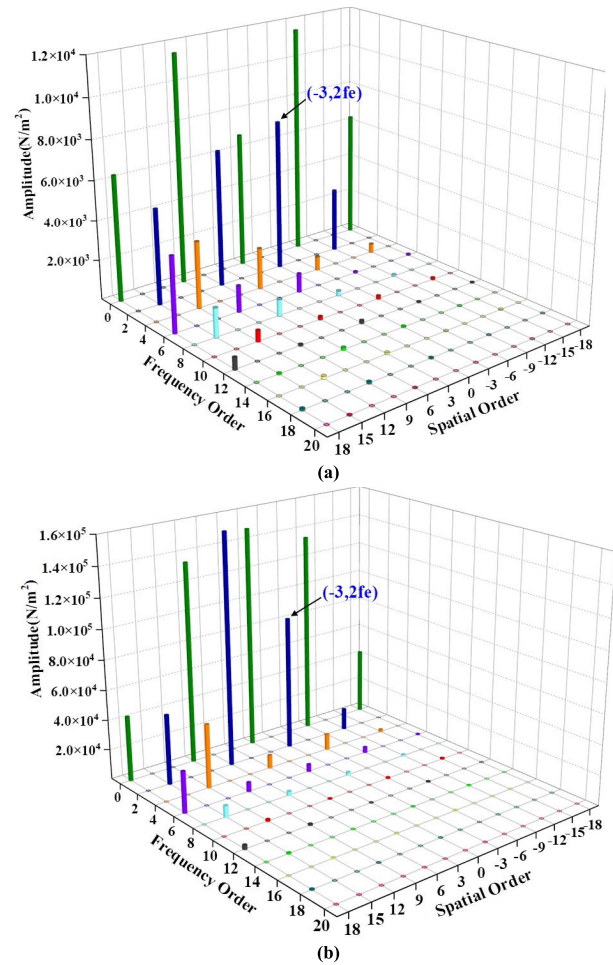


FIGURE 3. The distribution of AEFD under load. (a) Tangential. (b) Radial.

alent concentrated force and the equivalent torque are given by (9)-(11), respectively:

$$F_{r,z}(z) = \int_{\theta_z - \Delta\theta}^{\theta_z + \Delta\theta} LR_{is} [p_r \cos(\theta_z - \theta) + p_\tau \sin(\theta_z - \theta)] d\theta \quad (9)$$

$$F_{\tau,z}(z) = \int_{\theta_z - \Delta\theta}^{\theta_z + \Delta\theta} LR_{is} [p_\tau \cos(\theta_z - \theta) + p_r \sin(\theta_z - \theta)] d\theta \quad (10)$$

$$M_z(z) = \int_{\theta_z - \Delta\theta}^{\theta_z + \Delta\theta} LR_{is}^2 p_\tau \cos(\theta_z - \theta) d\theta \quad (11)$$

where L is the stacking length of the stator iron core, R_{is} is the stator inner radius, z is the tooth sequence, θ_z is the position of the z -th tooth. $F_{r,z}(z)$, $F_{\tau,z}(z)$, and $M_z(z)$ represent the equivalent concentrated force, tangential force and torque of the z -th tooth, and $\Delta\theta$ is the tooth pitch.

By substituting (8) into (9), the radial component of the ECF can be obtained [14], the radial component of the ECF

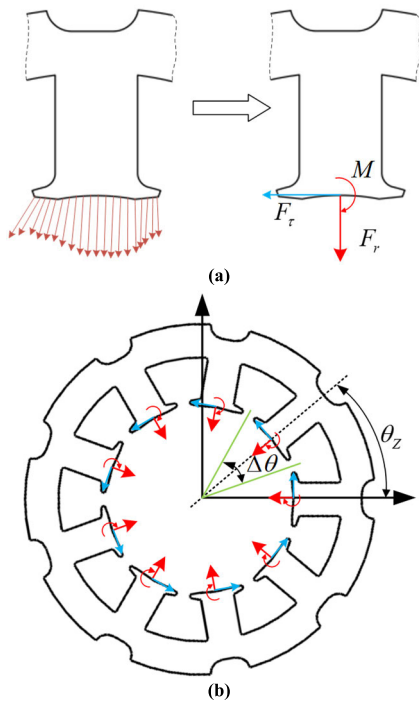


FIGURE 4. Equivalent model of distributed Aefd. (a) Force conversion model. (b) ECF model.

as follow:

$$\begin{aligned}
 F_{r,n,z} &= \frac{2LR_{is}\sigma_{n,f_n}^r}{n} \sin\left(\frac{n\pi}{Z_1}\right) \cos(2\pi f_n t - n\theta_z + \varphi_{n,f_n}^r) \\
 &= 2LR_{is} \frac{\sin(n\pi/Z_1)}{n} \sigma_{n,f_n}^r \cos(2\pi f_n t - n\theta_z + \varphi_{n,f_n}^r) \quad (12)
 \end{aligned}$$

Similarly, the tangential ECF is given by (13).

$$\begin{aligned}
 F_{\tau,n,z} &= \frac{2LR_{is}\sigma_{n,f_n}^\tau}{n} \sin\left(\frac{n\pi}{Z_1}\right) \cos(2\pi f_n t - n\theta_z + \varphi_{n,f_n}^\tau) \\
 &= 2LR_{is} \frac{\sin(n\pi/Z_1)}{n} \sigma_{n,f_n}^\tau \cos(2\pi f_n t - n\theta_z + \varphi_{n,f_n}^\tau) \quad (13)
 \end{aligned}$$

where $\theta_z = 2\pi z/Z_1, z = 1, 2, \dots, Z_1$, σ_{n,f_n}^r and σ_{n,f_n}^τ represent the amplitude of the radial and tangential Aefd harmonics with spatial n order and frequency f_n , $\varphi_{n,f_n}^r, \varphi_{n,f_n}^\tau$ is phase of Aefd harmonics.

In order to quantify the contribution of Aefd waves of different spatial orders to the vibration of the slotted stator, the tooth surface ECF model, as described by (12) and (13), reveals that the tooth modulation force is solely related to the amplitude of the Aefd and tooth modulation. Consequently, the concentrated force coefficient k_{ECF} is defined to decouple the contribution of tooth modulation and high-order force wave amplitude to the modulation force:

$$k_{ECF} = \sigma_{n,f_n} \times \frac{\sin(n\pi/Z_1)}{n} \quad (14)$$

where $|\sin(n\pi/Z_1)/n|$ represents the modulation of the stator teeth on the higher-order force waves, and the tooth modulation coefficient is used to measure its effect. This coefficient corresponds to different spatial orders of radial electromagnetic force waves. As illustrated in Fig. 5, the tooth modulation effect is nearly zero for the 125th-order. Therefore, force waves with spatial orders exceeding the 125th-order can be disregarded. Note that conclusion differs from the traditional perspective, which neglects the contribution of high-order force waves. This finding is derived by taking into account the high-order force modulation effect.

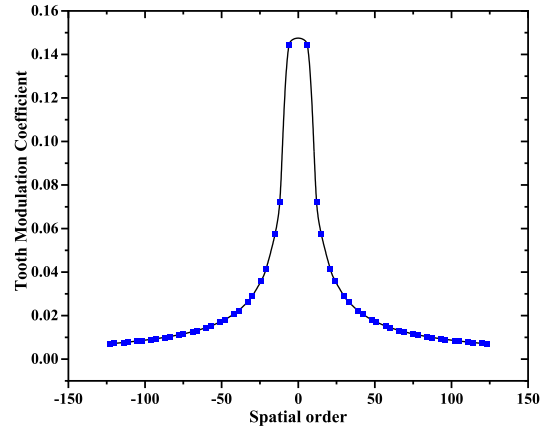


FIGURE 5. Tooth modulation coefficients of stator teeth for force waves of different spatial orders.

By substituting (14) into (12) and (13), it becomes evident that the amplitude of the ECF harmonic is determined by k_{ECF} , which is related to the product of the Aefd amplitude and the tooth modulation coefficient (k_{tooth}). As a result, a quantitative analysis of the contribution of different spatial order Aefd harmonics to the modulation of radial and tangential electromagnetic force waves after being modulated by teeth is possible. The radial and tangential ECF are given by (15).

$$\begin{aligned}
 F_{r,n,z} &= 2LR_{is}k_{ECF_r} \cos(2\pi f_n t - n\theta_z + \varphi_{n,f_n}^r) \\
 F_{\tau,n,z} &= 2LR_{is}k_{ECF_\tau} \cos(2\pi f_n t - n\theta_z + \varphi_{n,f_n}^\tau) \quad (15)
 \end{aligned}$$

where k_{ECF_r} and k_{ECF_τ} represent the radial and tangential concentrated force coefficients of the concentrated force harmonic, respectively.

It's important to note that for motors with varying pole-slot combinations, the distribution characteristics of Aefd harmonics and tooth modulation coefficients can differ significantly. Therefore, when determining the maximum order of Aefd harmonic components for typical cases, it becomes necessary to take into account the product of the amplitude of Aefd harmonics and the tooth modulation coefficients. This is due to the fact that when evaluating the impact of Aefd at different spatial orders on motor vibrations, the process involves acquiring normalized modulating forces through force transformation models. Subsequently, the modulating force amplitudes are compared to gauge the contributions of Aefd harmonic components at different orders to motor deformations.

D. HIGHER-ORDER FORCE WAVE MODULATION EFFECT

The electromagnetic vibration of the motor originates from the periodic deformation of the stator yoke, which is caused by the electromagnetic force acting on the stator teeth. By equating the distributed nodal forces on the stator teeth to a concentrated force, it becomes evident that the electro-magnetic force wave on the stator yoke is obtained by collecting the distributed electromagnetic force wave in the air gap through Z_1 stator teeth. This phenomenon is similar to signal acquisition. The Nyquist-Shannon sampling theorem states that when the sampling frequency is less than twice the maximum frequency component of the sampled signal, the sampled signal will experience distortion, meaning that high-frequency signals will be sampled as low-frequency signals. According to this principle, it can explain the behavior of high spatial order electromagnetic force harmonics inducing low-order modal vibrations in the stator. Additionally, through the ECF model, we can understand the regularities of high spatial order electromagnetic modulation. By comparing the harmonics of electromagnetic forces at different spatial orders when modulated into the same order of harmonic force amplitude, we can identify the key two-dimensional electromagnetic force harmonic components that dominate the motor vibration. The number of samples for θ_z in (12) and (13) is Z_1 , which represents the number of stator teeth. The sampling length is 2π , corresponding to the period of the spatial harmonic force of the electromagnetic force. Its spatial order is denoted by n , as shown in (16) and (17). Through discrete sampling by teeth, (16) and (17) can be derived, where the positive and negative signs of spatial order $(n - kZ_1)$ indicate whether the sampled force wave rotates in the same or opposite direction as the fundamental wave:

$$F_{r,n,z} = 2LR_{is}k_{ECF_r} \cos [2\pi f_n t - (n - kZ_1)\theta_z + \varphi_{n,r}] \quad (16)$$

$$F_{\tau,n,z} = 2LR_{is}k_{ECF_\tau} \cos [2\pi f_n t - (n - kZ_1)\theta_z + \varphi_{n,\tau}] \quad (17)$$

When the spatial order of the distributed electromagnetic force in the air gap does not satisfy the sampling theorem, the ECF harmonic will contain the Nyquist frequency. This means that the n -th order higher-order force wave will be modulated into a $(n - kZ_1)$ -th order lower-order force wave. However, the frequency of the force wave remains unchanged. That is, the force wave modulation effect only affects the spatial order of higher-order force waves. The law governing its force wave order is shown in (18):

$$||n| - kZ_1| \leq \frac{Z_1}{2} \quad (18)$$

When the spatial order of the AEFD harmonics collected by the stator teeth exceeds twice the number of stator teeth, high-order force waves will produce an effect equivalent to low-order force waves. This is known as aliasing, which occurs when the order n of the AEFD harmonic is greater than the Nyquist frequency $Z_1/2$. The spatial order of the concentrated force harmonics obtained by sampling will contain the Nyquist frequency, meaning that the spatial order of the collected concentrated force harmonics is $|n - kZ_1|$.

For example, two radial AEFD harmonics with spatial orders of 3rd and 6th in a motor, respectively. The 6th-order high-order force wave is modulated into a 3rd-order low-order force wave by the stator teeth through ECF model, as shown in Fig. 6. This phenomenon, where high-order force waves are modulated into low-order force waves by stator teeth, is called the modulation effect of high-order force waves or simply the force modulation effect.

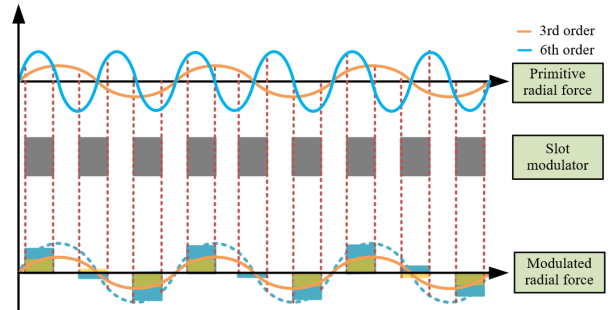


FIGURE 6. Modulation process of 3rd and 6th-order radial force.

The traditional method [7] equates the motor stator slotting model to a toothless model. This method estimates the influence of the spatial order of electromagnetic force waves on vibration deformation, as demonstrated in (19). Under the approximation the wave number of the deformation shape is the same as that of the radial force, simplified as shown in (20). It is found that the displacement is inversely proportional to the fourth power of the spatial order n of electromagnetic force, and posits that the contribution of high-order force waves to vibration can be disregarded.

$$\begin{cases} Y_{m,f_n}^s (m = 0) = \frac{R_{is}R_{yoke}}{Eh_{yoke}} p_{r,n,f_n}, & (n = m) \\ Y_{m,f_n}^s (m \geq 2) = \frac{12R_{is}R_{yoke}^3}{Eh_{yoke}^3(n^2 - 1)^2} p_{r,n,f_n}, & (|n| = m) \\ Y_{m,f_n}^d = Y_{m,f_n}^s \left[\left(1 - f_{n,f_n}^2 / f_m^2\right)^2 + 4\xi_m^2 f_{n,f_n}^2 / f_m^2 \right]^{-1/2}, & (n = m) \end{cases} \quad (19)$$

where Y_{m,f_n}^s and Y_{m,f_n}^d are the static and dynamic vibration displacements respectively, R_{yoke} , R_{is} and h_{yoke} are the average radius, inner diameter stator and thickness of the stator yoke respectively, p_{r,n,f_n} , n , and f_n are the amplitude, order and frequency of the radial force wave respectively. f_m and ξ_m are the eigenfrequency and damping ratio of the m -th order modal respectively.

$$Y_{m,f_n}^s (m \geq 2) \propto \frac{1}{n^4}, (n = m) \quad (20)$$

Under the motor's load condition, Fig. 7 depicts the harmonic component of the radial AEFD with an excitation

frequency of $18f_e$. Adhering to the previous perspective that low-order radial force waves primarily govern motor vibration, it would be assumed that the excitation source of the $18f_e$ frequency originates from the contribution of the same frequency 3rd-order radial AEFD (where f_e represents the fundamental frequency of the current).

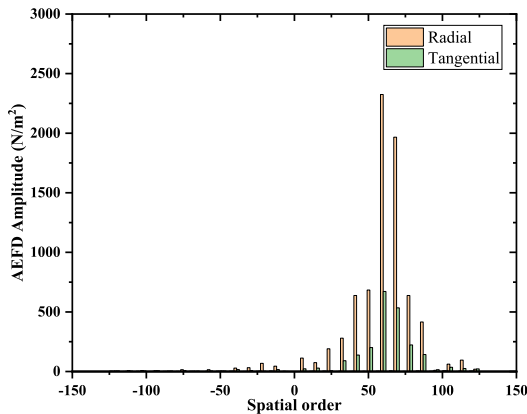


FIGURE 7. Harmonic content of $18f_e$ frequency component of radial AEFD under load condition.

However, the radial force wave component of the 3rd-order $18f_e$ is nearly zero, making it challenging to excite motor vibration. In contrast, higher-order force wave components (such as the 60th and 69th-order) possess amplitudes significantly larger than the radial force components of low-order force waves. Through the force modulation effect, it becomes evident that high-order force waves, when modulated into low-order forces by stator teeth, can also induce low-order modal vibrations in motors. Therefore, employing traditional methods to estimate the order of electromagnetic force waves on motor deformation proves unsuitable for FSCW motors, as high-order force waves can produce equivalent effects to low-order force waves under the modulation effect of stator teeth.

According to Fig. 5, it's evident that the AEFD harmonic modulation coefficients for orders exceeding 125th are less than 0.001. Additionally, In Fig. 7 the AEFD harmonic components of the motor at the $18f_e$ frequency are primarily concentrated around the 69th order, and the amplitudes of AEFD harmonics exceeding the 125th order are also very small. Consequently, this leads to the modulation force amplitude generated by AEFD orders beyond the 125th order being less than 1 N, rendering the influence of these higher-order harmonics negligible. Therefore, when assessing the contribution of different AEFD harmonic orders to vibration at a frequency of $18f_e$, considering AEFD harmonic orders up to the 125th is adequate for an accurate analysis.

The radial concentrated force is obtained by integrating the distributed AEFD on the stator teeth. By sampling a finite number of stator teeth, the results demonstrate that when the order of the 3rd-order force wave is less than $Z_1/2$ stator teeth, it maintains the same spatial order. Conversely, when the order of the 6th-order force wave is greater than $Z_1/2$ stator

teeth, it is modulated into a 3rd-order radial force harmonic. Fig. 3(b) illustrates the spatiotemporal distribution of radial AEFD waves with spatial orders that are multiples of 3. Fig. 8 presents the spatiotemporal distribution of radial concentrated force waves with force wave orders that are all less than $Z_1/2$ and only contain 0th and 3rd-order force waves. This observation also corroborates the spatial distribution law of radial concentrated force in (18), all high-order AEFD waves of this motor are modulated into 0th or 3rd-order force waves by stator teeth. The finding suggests that this type of motor exhibits a strong modulation effect, the resulting modulation vibration significantly contributes to the motor's vibration. Consequently, the modulation effect of high-order force waves cannot be overlooked.

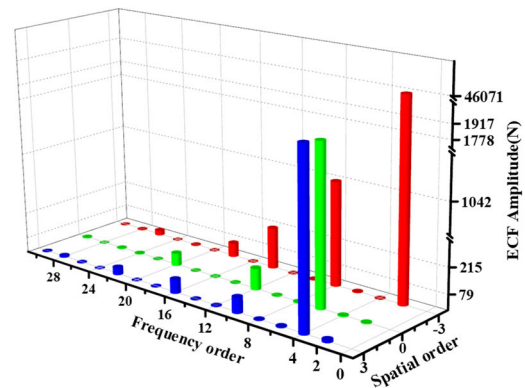


FIGURE 8. The distribution of radial ECF under load conditions.

In the 9S6P motor, all high-order radial AEFD waves are modulated into 0th or 3rd-order force waves. Similarly, when the pole-slot combination of the motor satisfies (21), the motor exhibits a strong modulation effect of high-order force waves, significantly contributing to the motor's vibration. For instance, the modulation force harmonic component of the 12S8P motor only contains 4th-order force waves, while the 12S10P pole-slot combination includes 2nd, 4th, and 6th-order components. Therefore, the modulation force effect of 12S8P is stronger than that of 12S10P motor, with the former belonging to the category of strong modulation effect motors.

$$2 \times r_{min} > \frac{Z_1}{2} \tag{21}$$

where r_{min} represents the minimum non-zero force wave order of the motor as the greatest common divisor of the number of teeth and poles of the motor, with $r_{min} = \text{GCD}(Z_1, 2p)$.

When the pole-slot combination of the motor aligns with the strong high-order force modulation effect, all high-order forces in the air gap are modulated by the stator teeth to the 0th and the smallest non-zero spatial order. This results in the superposition of high-amplitude high-order force harmonic components in the air-gap electromagnetic force, contributing to stator deformation. Therefore, considering the low-mode deformations induced by high-order forces can significantly enhance the precision of motor vibration analysis.

III. MODAL ANALYSIS AND MODEL EQUIVALENCE

To swiftly predict the vibration response of a motor under electromagnetic force excitation, it is essential to accurately obtain the motor’s modal parameters. This lays the foundation for the subsequent calculation of the motor’s vibration response using the modal superposition method. Initial values for the core and windings are set in the FE equivalent model, as displayed in Table 3. The outcomes of the FE modal simulation are presented in Table 4. The error between simulation and experiment exceeds 10%, indicating that employing actual material parameters of the components as the equivalent material parameters does not align well with experimental results. Therefore, to accurately predict the motor’s vibration behavior, further adjustments to the material properties of the FE equivalent model are required.

TABLE 3. Initial values of material parameters.

Items	Core	Winding
Density (kg/m ³)	$\rho = 7268$	$\rho = 3200$
Young’s modulus (Gpa)	$E = 206$	$E = 0.3$
Poisson’s ratio	$\nu = 0.3$	
Shear modulus (Gpa)	$G = 79.23$	$G = 0.15$

A. MODAL EXPERIMENT

Fig. 9(a) illustrates the modal test by hammer impact method for stator core and stator assembly, which is suspended by an elastic rope to simulate an unconstrained state. For the modal test, two accelerometers are mounted on the surface of the stator core and three groups (equally spaced axially) of 27 points (uniformly distributed around) are arranged for impact excitation. Fig. 9(b) presents the constructed experimental node model of the stator core.

In the modal test, a hammer is utilized to excite the free vibration of the component being tested at each designated point, triaxial PCB accelerometers are used to obtain the response signals of the stator core at different impact points. Subsequently, the vibration and force signals are input into LMS Test Lab software, resulting in the acquisition of the modal state of the tested components. Modal parameter estimation and identification were carried out using the Poly-max tool. Based on this hammer impact method, the corresponding modal parameters of the stator core and stator assembly are presented in Tables 5 and 6, respectively.

TABLE 4. Errors in modal simulation and modal testing.

Mode Order		2	3	4
Measured (Hz)	Core	1559.8	3929.4	6546.4
	Assembly	1282.1	2794.1	--
Simulated (Hz)	Core	1709.6	4389.4	7255.1
	Assembly	1417.8	3564.1	8519.3
Error (%)	Core	-9.6	-11.7	-10.8
	Assembly	-10.6	-27.5	--

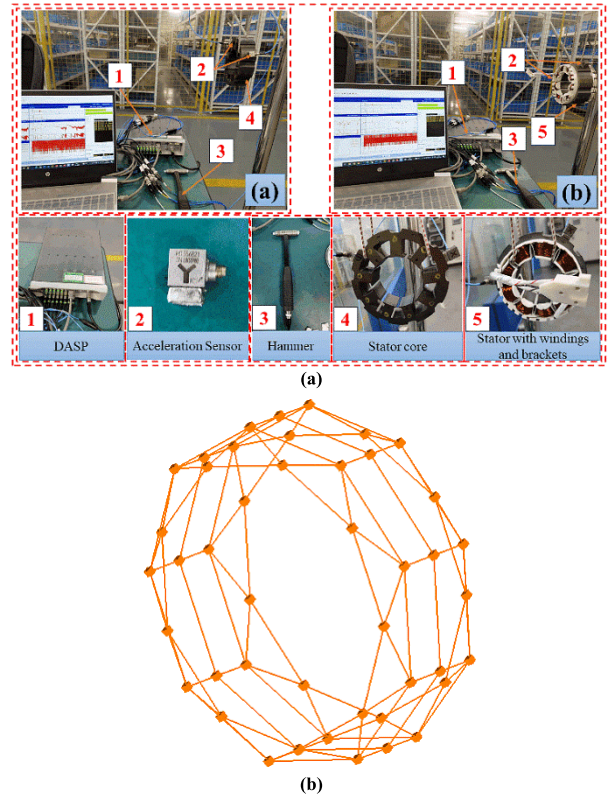


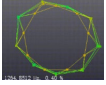
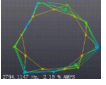
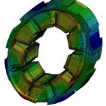
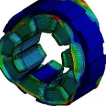
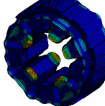
FIGURE 9. Modal tests. (a) Schematic diagram. (b) Node layout.

TABLE 5. Measured and simulated modals of stator core.

Mode Order		2	3	4
Measured	shapes			
	frequency (Hz)	1559.8	3929.4	6546.4
Simulated	shapes			
	frequency (Hz)	1554.1	3936.6	6529.2
Relative error (%)		0.36	0.18	0.26

In Table 6, experimental data for the 4th-order mode of the stator assembly were not obtained. We conducted a retest of the experimental data, which closely matched the results of the original modal experiment. As a result, we confirmed the accuracy of the modal experiment. Subsequently, combining the 4th-order modal data obtained from FEA, we determined that the modal frequency of the stator assembly was 8247.1Hz. However, the modal testing instrument used in the impact test has a measurement frequency range of up to 8000Hz, and the 4th-order modal frequency of the stator assembly exceeded this maximum range. This is the reason

TABLE 6. Measured and simulated modals of stator assembly.

Mode Order		2	3	4
Measured	shapes			--
	frequency (Hz)	1282.1	2794.1	--
Simulated	shapes			
	frequency (Hz)	1282.9	2815.1	8247.1
	Relative error (%)	-0.06	-0.75	--

why the modal experiment did not capture the 4th-order modal of the stator assembly.

B. EQUIVALENT FINITE ELEMENT MODEL

In FE modeling of motor stator and winding structures, accurately representing the actual structure through detailed modeling can be challenging. As such, equivalent modeling of the stator core and winding is essential for simulating the motor’s structural characteristics and predicting its vibration behavior accurately. For conventional structures, such as compressor casings and simple insulating bracket models, modeling can be based on actual conditions. However, due to the significant differences in material parameter properties of the motor stator core in axial and radial planes, the stator core can be equivalently modeled as a continuous elastic body with orthotropic material parameters. When establishing the winding FE model, the internal structure of the winding is not considered, and it is assumed that the stator teeth and winding are in close contact. The winding, tightly wound within the stator tooth slot and fixed by insulation bracket, can be equivalently modeled as a continuous elastomer with orthotropic material parameters for simplified FE modeling [31], [32].

C. CALIBRATION OF ANISOTROPY PARAMETERS

Orthotropic material properties encompassing a total of nine parameters: $E_x, E_y, E_z, G_{xy}, G_{yz}, G_{zx}, \nu_{xy}, \nu_{yz}$ and ν_{zx} . According to the symmetry of orthogonal planes, as demonstrated in (22).

$$E_x = E_y, G_{yz} = G_{zx}, \nu_{yz} = \nu_{zx} \tag{22}$$

Among the elastic modulus, shear modulus and Poisson’s ratio, only two are entirely independent [33]. Consequently, the G_{xy} and G_{yz} parameters can be derived from E_x, E_z, ν_{zx} and ν_{yz} , as shown in (23).

$$G_{xy} = \frac{E_x}{2(1 + \nu_{xy})}, G_{yz} = \frac{E_y}{2(1 + \nu_{yz})} = G_{zx} \tag{23}$$

To converge the FE modal simulation results with the experimental measurements and obtain a high-precision equivalent model of the motor, it is essential to calibrate the

material parameters of the equivalent model. Fig. 10 presents a flowchart for correcting the orthotropic material parameters of the stator core.

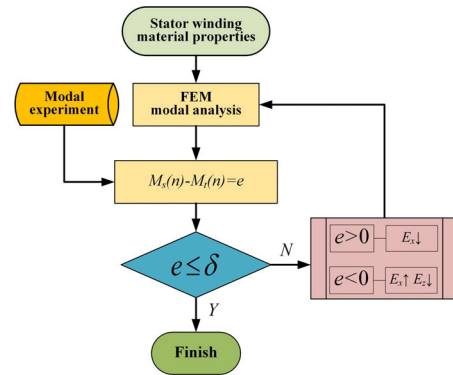


FIGURE 10. Stator core material parameter correction flowchart.

The revised material parameters of motor components are presented in Table 7 while the modal simulation of the stator core and stator assembly equivalent models is depicted in Tables 5 and 6, respectively. The error between the FE modal simulation and modal test is controlled within 1%, indicating that the calibrated FE equivalent model can accurately predict the dynamic characteristics of the motor stator. The Compressor Motor assembly is assigned calibrated material properties. The main modes of the compressor motor assembly, obtained through FE modal simulation, are shown in Fig. 11 with the third-order mode being the primary source of vibration.

TABLE 7. Modified, bracket and housing material properties.

Items	Density (kg/m ³)	Young’s Modulus (Gpa)	Poisson’s Ratio	Shear Modulus (Gpa)
Stator core	$\rho = 7268$	$E_x = E_y$	$\nu_{xy} = \nu_{yz}$	$G_{yz} = G_{zx}$
		$= 190$	$= \nu_{zx}$	$= 88$
		$E_z = 180$	$= 0.3$	$G_{xy} = 98$
Solt winding	$\rho = 4297$	$E_x = E_y$	$\nu_{xy} = \nu_{yz}$	$G_{yz} = G_{zx}$
		$= 0.4$	$= \nu_{zx}$	$= 0.153$
		$E_z = 0.5$	$= 0.3$	$G_{xy} = 0.192$
End winding	$\rho = 4297$	$E_x = E_y$	$\nu_{xy} = \nu_{yz}$	$G_{yz} = G_{zx}$
		$= 0.5$	$= \nu_{zx}$	$= 0.072$
		$E_z = 0.4$	$= 0.3$	$G_{xy} = 0.185$
Bracket	$\rho = 1205$	$E = 0.193$	$\nu = 0.39$	$G = 0.0694$
Housing	$\rho = 7850$	$E = 200$	$\nu = 0.3$	$G = 76.92$

The revised material parameters of motor components are presented in Table 7 while the modal simulation of the stator core and stator assembly equivalent models is depicted in Tables 5 and 6, respectively. The error between the FE modal simulation and modal test is controlled within 1%, indicating that the calibrated FE equivalent model can accurately predict the dynamic characteristics of the motor stator. The Compressor Motor assembly is assigned calibrated material properties. The main modes of the compressor motor assembly, obtained through FE modal simulation, are shown in Fig. 11 with the 3rd-order mode being the primary source of vibration.

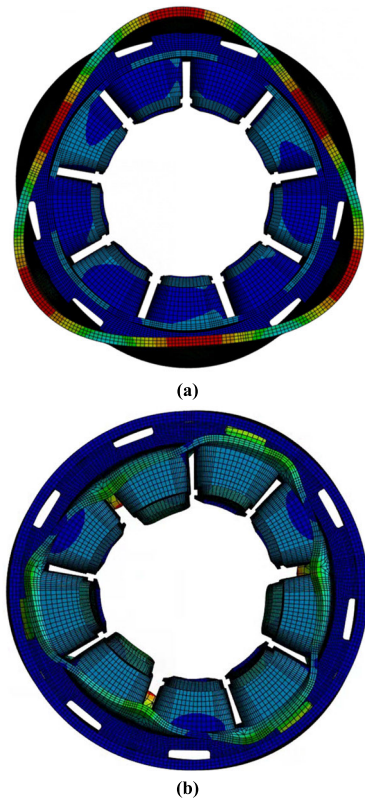


FIGURE 11. Compressor motor 3rd order mode. (a) Housing 3rd order (2193.3Hz). (b) Stator 3rd order (3202.7Hz).

Based on the actual structures of various motor components, we conducted corresponding anisotropic and isotropic equivalent modeling. Employing a trial-and-error approach, we refined the material parameters in the FE equivalent model to closely align the FE modal simulation results with the modal experiment outcomes, thereby achieving a highly precise FE equivalent model. Simultaneously, in terms of generality, we observed that the calibrated equivalent material parameters exhibit a degree of universality. When applied to equivalent models of motors with different pole-slot combinations but similar types, the obtained equivalent material parameters maintain a high level of accuracy. The error between FE equivalent model modal simulation results and modal experiment outcomes does not exceed 5%. This indicates that in the preliminary design and configuration of motors, the obtained equivalent material parameters can be efficiently and accurately used through FE methods to acquire the motor structure’s modal parameters, thereby expediting the iterative design and modal planning of the motor.

IV. VIBRATION NOISE ANALYSIS

In the conventional analysis of vibration, the impact of tangential AEFD on vibration is often overlooked, focusing solely on the low-order harmonic components of radial AEFD, as illustrated in Fig. 3. The more significant amplitude low-order electromagnetic force harmonic components

are the 3rd-order $2f_e$ frequency, which is generated by the interaction between the rotor’s primary pole magnetic field and the stator’s first-order tooth harmonic. This interaction serves as the primary source of motor vibration. This conclusion is reached by disregarding the influence of high-order force waves. According to (16)-(17), under the modulation effect of stator teeth on high-order force waves, the impact of high-order force waves on the stator is comparable to that of low-order force waves, potentially leading to low-order modal vibration [14], [15], [16], [17], [19]. Concurrently, the tangential AEFD exhibits the same spatial and temporal distribution as the radial AEFD, sharing similar characteristics in causing motor vibration. Fig. 12 demonstrates that high-order AEFD harmonics are modulated by stator teeth into low-order force waves. Both high-order and low-order radial and tangential force waves can induce low-order modal vibrations in motors.

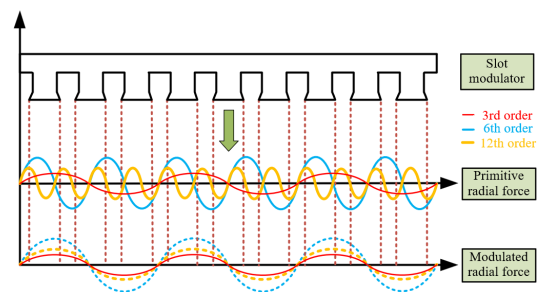


FIGURE 12. Modulation effect of high-order force waves of tangential force and radial force.

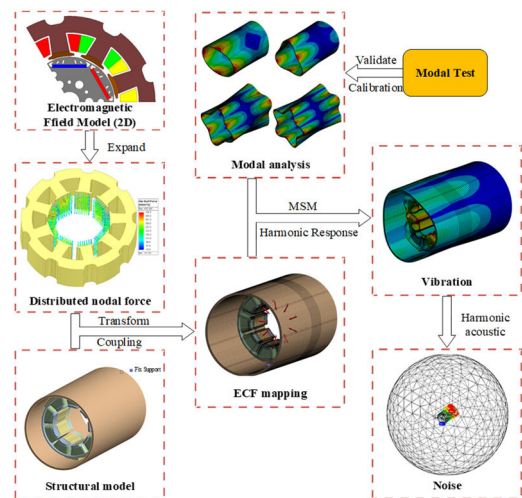


FIGURE 13. Flowchart of electromagnetic vibration and noise simulation of motor.

Waterfall analysis is a tool that is often used to evaluate the acoustic and/or vibratory performance of rotating machinery. Due to the wide operating speed range of the air-conditioning compressor motor, in order to identify the source of vibration and noise caused by harmonic components of electromagnetic forces, a multi-speed simulation

analysis was conducted. This analysis encompasses the vibration characteristics of the motor under no-load operating conditions, as well as the vibrations and noise generated under load operating conditions due to the separate actions of radial and tangential forces, along with their coupled interactions. The simulated rotational speed range spanned from 500 to 3000 rpm. The multi-physics coupling simulation process is illustrated in Fig. 13. Firstly, the radial and tangential nodal distribution of AEFD experienced by the stator teeth of the motor are computed using Maxwell 2D, and a three-dimensional distribution force is obtained through axial extension. This transient distribution force is transformed into a form of harmonic ECF and coupled to the structural field. Subsequently, a harmonic response simulation analysis of the assembled model of the stator and housing of the compressor motor is conducted using the modal superposition method.

The equivalent model material attributes for each part are aligned with the data calibrated in Section III of the modal experiments. This process facilitates the determination of the motor’s vibration response under the individual and combined effects of radial and tangential forces. In the pursuit of computing the noise generated by the compressor motor, the motor vibration velocity obtained from the harmonic response simulation is coupled into the harmonic acoustics. The noise solution is defined within a spherical domain with a radius of 1m centered on the motor, culminating in the generation of the noise response of the compressor motor.

As shown in Figs. 14, the predicted vibration waterfall map of the motor under no-load conditions is shown under the separate and coupled effects of radial and tangential forces, In Figs. 15-17, they respectively represent the predicted vibration noise waterfall map of the motor under load conditions under the separate and coupled effects of radial and tangential forces.

The vibration waterfall diagram obtained from simulation predictions under no-load conditions is shown in Figure 14. Comparing this with the vibration waterfall diagrams predicted under loaded motor conditions in Figures 15(a), 16(a) and 17(a), it can be observed that the vibrations under no-load conditions mainly consist of vibrations at $2f_e$ and $4f_e$ frequencies. Additionally, tangential forces enhance vibrations generated by radial forces, irrespective of whether the motor is loaded or not. However, under loaded conditions, the vibration frequency harmonics of the motor are more pronounced compared to no-load conditions. Therefore, the vibration characteristics of the motor are more effectively reflected under loaded conditions. As a result, we conducted an in-depth investigation into the effects of radial and tangential forces, as well as their coupled interactions, under loaded motor conditions.

A. RADIAL/TANGENTIAL ELECTROMAGNETIC FORCE ACTION

Fig. 15(a) reveals that when the radial force acts alone, the most pronounced vibrations occur at the 6th, 24th, and 66th orders, corresponding to $2f_e$, $8f_e$, and $22f_e$ frequency vibra-

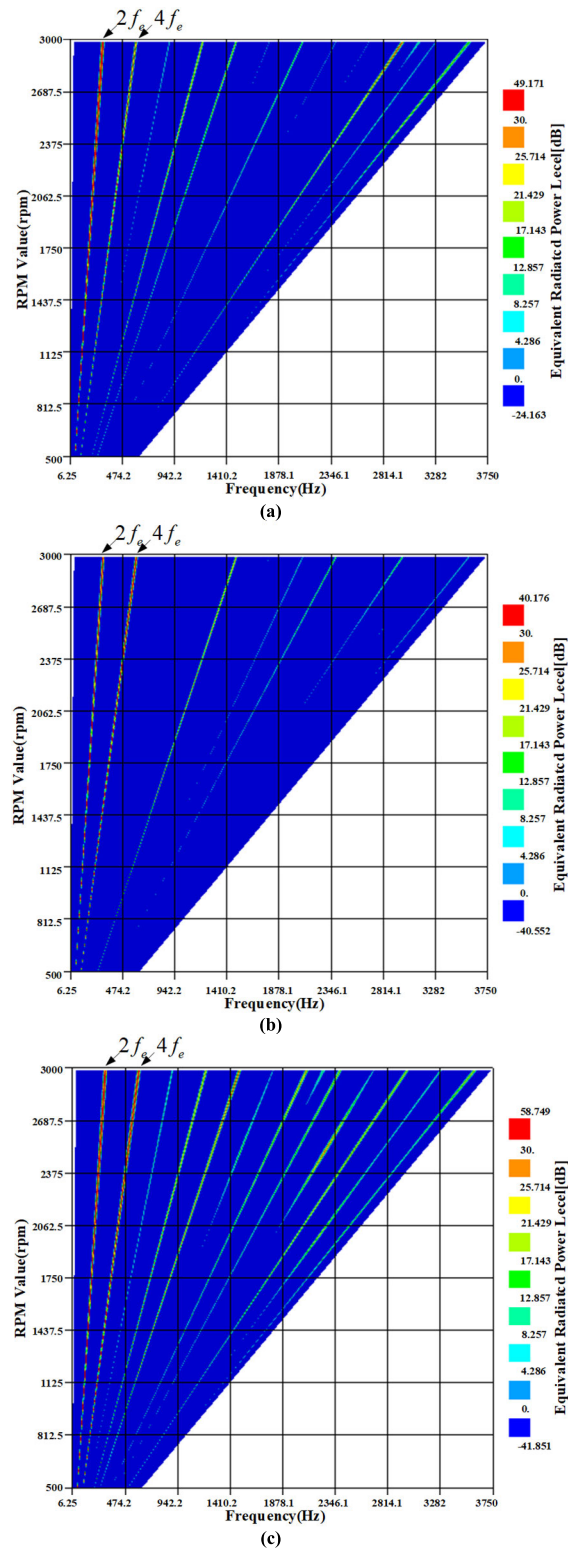
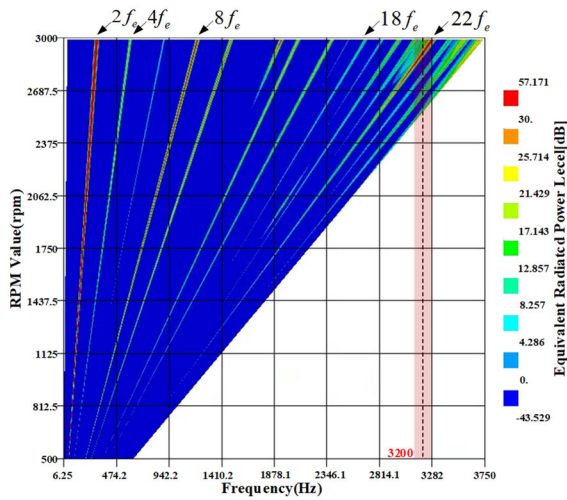
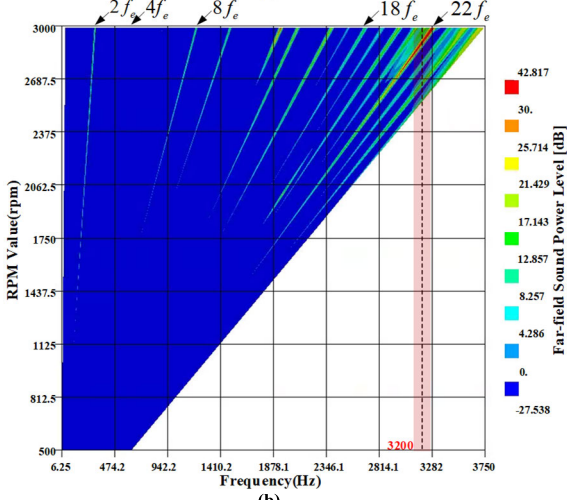


FIGURE 14. Vibration waterfall map of the motor under no-load conditions. (a) Radial force. (b) Tangential force. (c) Coupling force.

tions, respectively. As per (16) and (18), high-order force waves with frequencies of $2f_e$, $8f_e$ and $22f_e$ can also induce vibrations at these frequencies, since high-order force waves



(a)



(b)

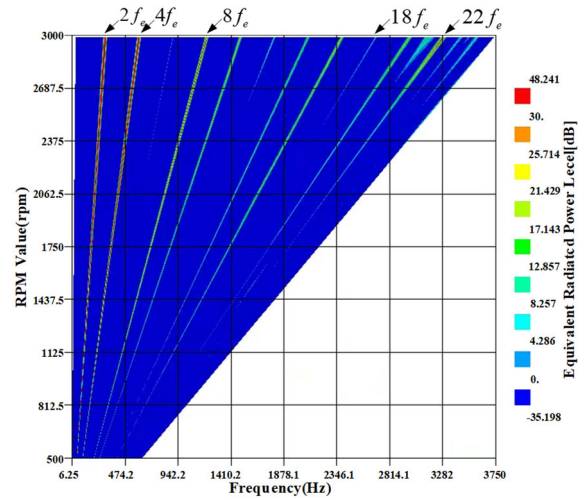
FIGURE 15. Vibration and noise waterfall map under the action of radial force during motor loading. (a) Vibration. (b) Noise.

can be modulated into low-order harmonic forces. The same time, a resonance band emerges near 3200Hz, which can be attributed to the radial force excitation order and frequency being proximate to the stator’s 3rd mode of 3202.7 Hz of the motor assembly. This results in resonance within the motor stator assembly, as depicted in Fig. 11(b).

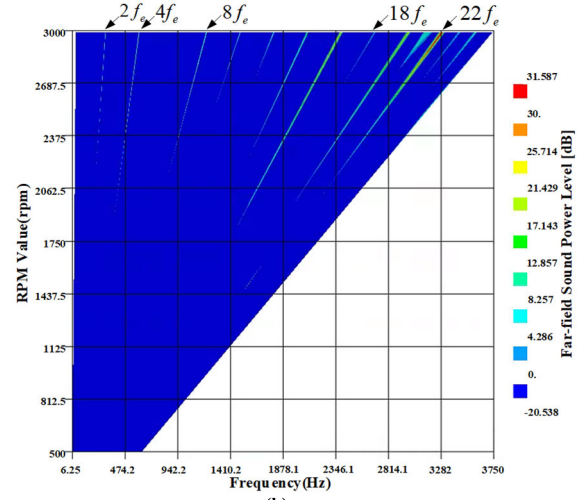
Furthermore, when the tangential force acts independently, as illustrated in Fig. 16(a), the primary vibration orders induced by the tangential force on the motor are the 6th, 12th, and 66th orders, corresponding to $2f_e$, $4f_e$, and $22f_e$ frequency vibrations, respectively. In this scenario, no resonance is observed.

B. ELECTROMAGNETIC FORCE COUPLING ACTION

When the radial and tangential force are coupled, the motor exhibits larger vibration orders at 6th, 12th, 24th, 30th, 54th and 66th orders, corresponding to $2f_e$, $4f_e$, $8f_e$, $10f_e$, $18f_e$, and $22f_e$ frequency vibrations, respectively. as shown in Fig. 17(a). Among these, the 6th and 54th orders are the



(a)



(b)

FIGURE 16. Vibration and noise waterfall map under the action of tangential force during motor loading. (a) Vibration. (b) Noise.

most pronounced, corresponding to $2f_e$, and $18f_e$, vibration frequencies. Simultaneously, a significant resonance band also appears near 2200Hz. This resonance results from the electromagnetic force wave order and frequency aligning with the 3rd-order mode of the motor assembly housing at 2193.3Hz, as depicted in Fig. 11(a). This observation suggests that when the radial force is excited alone, it induces the stator’s 3rd order modal resonance of the motor assembly. In contrast, when the radial force and tangential force act together, they induce the motor assembly housing and stator’s 3rd-order modal at 2200 Hz and 3200 Hz. The emergence of the 2200 Hz resonance is a consequence of the combined action of radial and tangential forces. Moreover, the $18f_e$ vibration frequencies of the motor under the coupling action of radial and tangential forces is larger than that under the action of radial force alone. This finding indicates that tangential force plays a crucial role in motor vibration. For this motor, considering only the effect of radial force would underestimate the actual vibration. In reality, as an

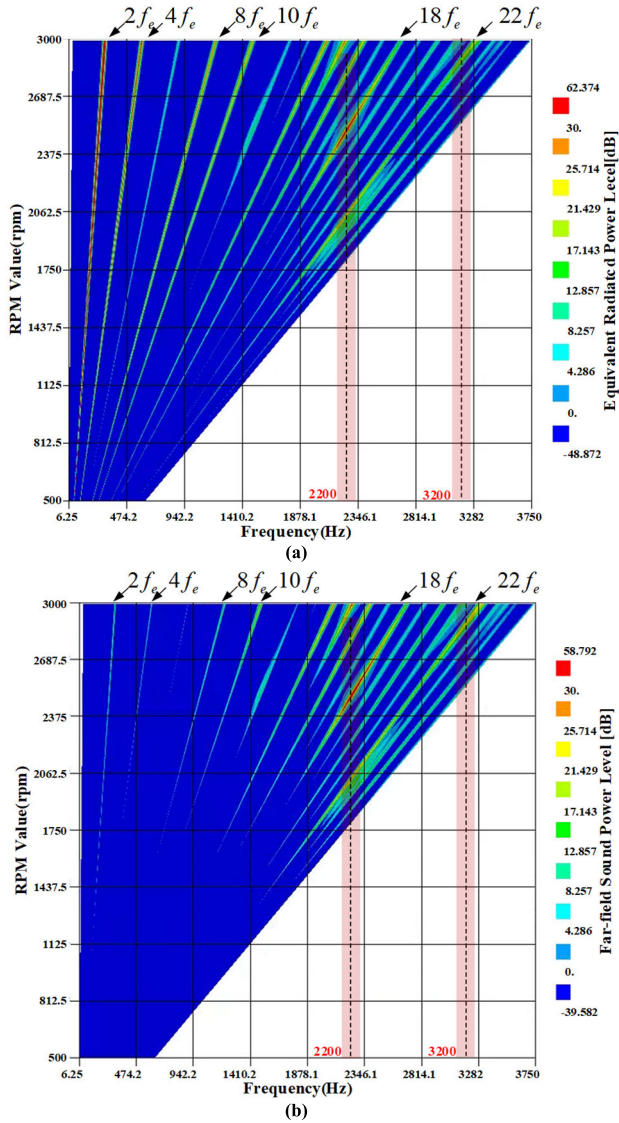


FIGURE 17. Waterfall map of vibration noise due to coupling of radial and tangential forces during motor loading. (a) Vibration. (b) Noise.

objectively existing local force, tangential force can either enhance or reduce vibrations caused by radial force [20]. Tangential electromagnetic force can also induce low-order modal deformation in motors. When tangential force is coupled with radial force, the presence of tangential force may either weaken or amplify vibrations caused by radial force, depending on the spatial phase difference between radial force wave and tangential force wave harmonics. The mechanism underlying this phenomenon will be investigated in greater detail in future work.

According to Figs. 15(b), 16(b) and 17(b), the noise characteristics of the motor are similar to its vibration characteristics. However, such as the 6th and 12th-order vibrations of the motor, corresponding to $2f_e$ and $4f_e$ frequency noise generated by low-order vibrations, are significantly smaller than the noise caused by the 3rd-order modal resonance of

the motor assembly. This suggests that motor resonance is the primary source of motor noise.

As a result, reducing the harmonic components of electromagnetic force that cause motor resonance can significantly decrease motor noise. Simultaneously, the most severe vibration noise of the motor is attributed to the $18f_e$ excitation frequency. Based on the force wave modulation rule, such as (18), it is evident that force waves higher than $Z_1/2$ order are modulated into 0th-order or 3rd-order force waves. The 0th-order modal frequency is significantly higher than the 3rd-order modal frequency and will not cause resonance within the motor’s operating speed range. Therefore, the vibration noise of the motor arises from the action of the 3rd-order modulation force, and high-order force modulation will not alter the frequency of AEFD. The vibration noise caused by this frequency order originates from different spatial orders of radial and tangential AEFD harmonics at $18f_e$ frequency. These harmonic forces are all modulated into 3rd- order modulation forces. Through (14), the contribution of different spatial order AEFD waves to vibration after tooth modulation can be quantified. By decoupling the tooth modulation coefficient and AEFD amplitude through the concentrated force coefficient, the influence of different spatial order AEFD on modulation force can be quantitatively analyzed. The process diagram for analyzing the crucial electromagnetic force harmonic components in motor vibration is depicted in Figure 18. The steps to determine the primary AEFD harmonic components that generate a specific modulation force harmonic component are as follows:

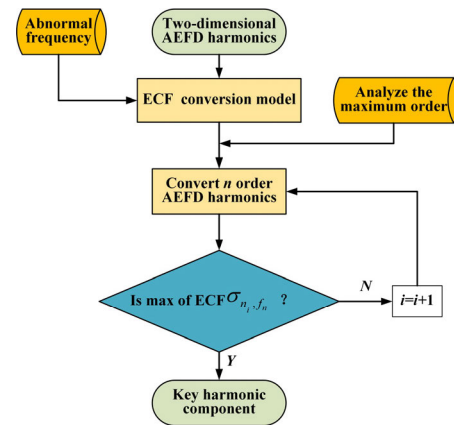


FIGURE 18. Flowchart for determining key two-dimensional electromagnetic force harmonics leading to motor vibration.

1. Determining the modulation force harmonic components: The modulation force harmonic frequency of the motor’s main vibration noise is $18f_e$. From Fig. 8, it is evident that the non-zero spatial order of the modulation force wave harmonic components of the motor is only 3rd-order. Therefore, the vibration noise of the motor is dominated by the 3rd-order $18f_e$ frequency modulation force harmonic.

- Determining the frequency order of AEFD: Since the modulation effect only has a modulation influences the spatial order of AEFD waves, the frequency of AEFD harmonic components that generate 3rd-order $18f_e$ modulation harmonic force is also $18f_e$.
- Determining the spatial order AEFD: According to the high-order force wave modulation rule (18), the spatial order of AEFD that generates 3rd-order modulation force satisfies $n' = \min(n \pm kZ_1)$. n' represents the spatial order of AEFD with spatial order n after tooth modulation. As shown in Table 8, these spatial order harmonic components of AEFD will all be modulated into 3rd-order modulation force waves.
- Determining the main harmonic components of AEFD causing vibration noise: According to (14), the ECF can decouple the amplitude of AEFD and tooth modulation coefficient. This allows for a quantitative analysis of the contribution of different harmonic components of AEFD to the 3rd-order modulation force.

TABLE 8. Satisfying 3rd order modulation harmonic force.

AEFD spatial Order	Tooth Modulation Coefficient	AEFD Amplitude (N/m ²)			
		Radial		Tangential	
		Forward	Reverse	Forward	Reverse
6/-6	0.1443	112.6579	2.1952	22.7150	0.4837
12/-12	0.0722	2.3261	44.6333	3.5089	16.4671
15/-15	0.0577	74.7187	4.6933	29.0712	2.4041
21/-21	0.0412	4.1391	69.0670	1.6334	2.5305
24/-24	0.0361	190.6939	2.1687	6.3835	4.2184
30/-30	0.0289	1.0888	32.0363	3.6123	8.3742
33/-33	0.0262	279.7051	1.0942	90.7822	0.9136
39/-39	0.0222	1.8054	28.7485	2.3851	16.0881
42/-42	0.0206	638.1996	3.1270	138.2857	3.7242
48/-48	0.0180	2.8669	4.3252	0.2644	3.8202
51/-51	0.0170	683.7558	3.6859	201.2023	3.7399
57/-57	0.0152	3.1101	15.6437	2.9064	5.1741
60/-60	0.0144	2324.9159	0.3885	671.8987	2.6152
66/-66	0.0131	5.8751	1.8260	2.7543	3.4135
69/-69	0.0126	1966.7869	2.5682	534.1263	2.8139
75/-75	0.0115	1.3987	15.3795	0.4150	7.8789
78/-78	0.0111	637.7918	2.0785	222.7579	1.2280
84/-84	0.0103	5.2755	3.6206	3.1980	4.4703
87/-87	0.0100	416.0398	1.5898	142.3586	1.7069
...

Figs. 19(a) and 20(a) show that high-order force wave components have amplitudes much larger than those of low-order force waves for spatial orders within 125 orders. Tooth modulation coefficients for spatial orders exceeding 125 are very small, and higher-order contributions can be ignored. Figs. 19(b) and 20(b) illustrate the magnitude of the corresponding 3rd-order modulation force amplitude generated by AEFD under tooth modulation. The larger the modulation force amplitude, the greater the contribution. In combination with the modulation force amplitude, it can be determined that the $18f_e$ frequency vibration noise present in the motor is contributed by the 3rd-order $18f_e$ frequency modulation force. Its main sources of contribution are successively the coupling effects of radial and tangential AEFD harmonic

components of 69th-order $18f_e$, 60th-order $18f_e$, and 6th-order $18f_e$ frequency.

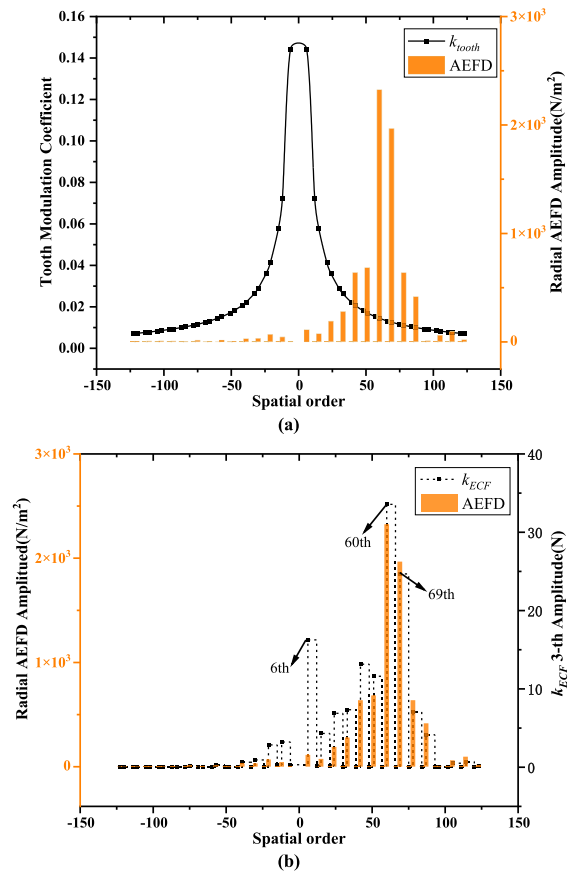


FIGURE 19. Contribution of radial AEFD harmonics. (a) Tooth modulation coefficient and $18f_e$ frequency radial AEFD. (b) $18f_e$ frequency radial AEFD and 3rd-order radial ECF.

Through multi-physics coupling simulations, it is evident that the motor exhibits abnormal vibration noise at the $18f_e$ frequency. If traditional methods were employed, it would be assumed that the 3rd order $18f_e$ frequency radial electro-magnetic force harmonic component is the primary source of this vibration. However, its magnitude is less than 1 N/m^2 , making it challenging to excite the $18f_e$ frequency vibration in the motor. Therefore, the conclusion that low spatial order harmonic electromagnetic forces dominate motor vibration has limitations. In our proposed method, we comprehensively consider the influence of high spatial order electromagnetic force harmonics and the combination of radial and tangential electromagnetic forces on motor vibration. Through FE multi-physics coupling simulations, we analyze motor vibration and discover that the abnormal vibration in the studied motor at the $18f_e$ frequency primarily results from the coupling interaction of 69th, 60th, and 6th harmonic electromagnetic force components at the same frequency in the radial and tangential electromagnetic forces. Traditional analysis methods cannot adequately explain this phenomenon, indicating that disregarding the contributions of high-order electromagnetic force harmonic components

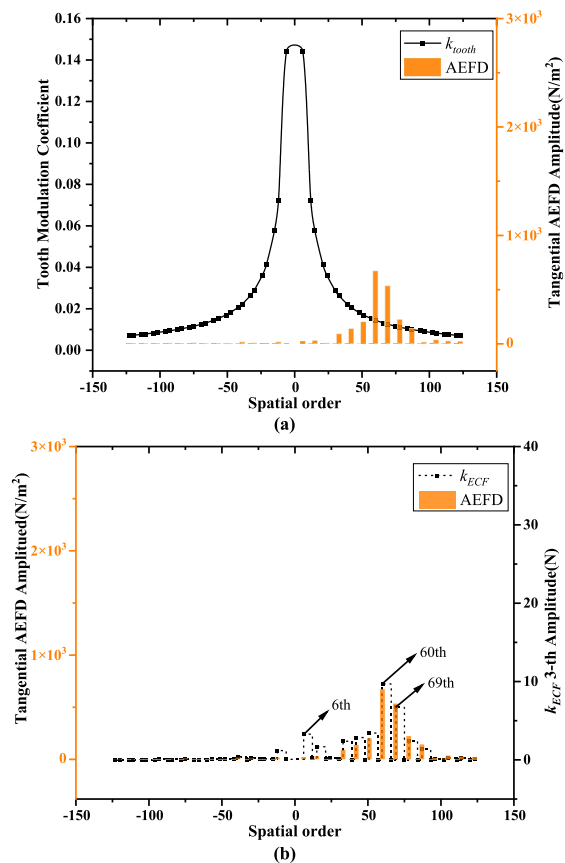


FIGURE 20. Contribution of tangential AEFD harmonics. (a) Tooth modulation coefficient and $18f_e$ frequency tangential AEFD. (b) $18f_e$ frequency tangential AEFD and 3rd-order tangential ECF.

and tangential forces to motor vibration in accordance with traditional methods limits the analysis of motor vibration. Additionally, this also reflects that our proposed method can accurately capture the critical two-dimensional harmonic components of electromagnetic forces responsible for motor vibration.

In the motor design phase, the critical consideration is the selection of appropriate slot-pole combinations. This is because the relationship between the stator slot number and the minimum non-zero spatial order force wave directly impacts whether there is a high-order force modulation effect in the slot-pole combination. In the vibration analysis of the motor, when the slot-pole combination satisfies the high-order force modulation effect, considering the contribution of high spatial order electromagnetic force harmonics to motor vibration is highly effective in enhancing the accuracy of motor vibration analysis.

In fact, the modulation force decoupling model serves the purpose of identifying the critical AEFD harmonic components that dominate electromagnetic vibrations. In future efforts to optimize motor vibrations, the identification of these key two-dimensional electromagnetic force harmonic components obviates the need for multi-physics coupled simulations to calculate motor vibrations. This is achieved by

optimizing motor vibrations through the reduction of amplitude in the critical electromagnetic force harmonics. Due to the fact that the ECF is a quadratic integral term of air gap magnetic density, variations in stator slot parameters are sensitive to the modulation force decoupling model. Analyzing the accuracy of the modulation force decoupling model in different scenarios can be accomplished by comparing various concentrated force equivalent mapping methods. For instance, comparing nodal forces based on the virtual work method or distributed forces based on the Maxwell stress tensor method. Through a unified calculation and comparison of the ECF force using these two methods, their relative error falls within 10%, indicating an acceptable level of accuracy for the model [19].

V. CONCLUSION

This paper proposes a novel method for the precise identification of the essential two-dimensional harmonic components within AEFD responsible for motor vibration noise. This method takes into consideration the phenomenon of high-order AEFD affecting the stator slot structure, which in turn induces low-order modal vibrations in the motor. Additionally, it accounts for the influence of tangential AEFD on motor vibrations. The study commences by investigating the modulation patterns of high-order forces using the ECF model. Subsequently, a quantitative analysis method is introduced to assess the contribution of high-order forces to the modulation force, thereby determining the impact of different spatial-order AEFD harmonics on motor vibrations. To support these analyses, an equivalent and simplified motor FE model is established, and high-precision motor FE models are calibrated through modal experiments. Following this, the paper explores the influence of tangential forces on motor vibration noise using a multi-physics field-coupling simulation approach. Finally, a modulation force decoupling model is employed to identify the key AEFD harmonics, offering theoretical insights and practical significance for the accurate identification of the source of motor electromagnetic vibration noise. The primary conclusions drawn in this paper are as follows:

- 1) When high-order air-gap electromagnetic forces act on the stator slot structure, the modulated low-order forces are confined within the $Z_1/2$ -th order. For motors with different pole-slot combinations, recognizing the impact of high-order forces inducing low-order modal vibrations in the motor can significantly enhance the accuracy of motor vibration analysis.
- 2) In instances where the motor exhibits a notable high-order force modulation effect and enters into resonance, high-order AEFD harmonic components emerge as the principal source of vibration noise.
- 3) The combined influence of radial electromagnetic forces and tangential electromagnetic forces can intensify vibrations generated by radial forces. Disregarding the contribution of tangential electromagnetic forces may result in an underestimation of motor vibration noise.

4) A new method is proposed for the decoupling of tooth modulation and AEFD amplitude through the concentrated force coefficient. This approach enables a quantitative analysis of the contribution of the force wave modulation effect to the modulation force.

5) The critical electromagnetic force harmonics responsible for the abnormal $18f_e$ frequency vibration noise in this motor are identified as the 3rd-order $18f_e$ modulating forces resulting from the modulation of 69th, 60th, and 6th-order harmonics of both radial and tangential AEFD at the same frequency.

In future research, we will direct our focus towards examining the impact of various factors including IPMSM motor drives, rotor tilt eccentricity, and the phase of tangential electromagnetic forces on motor vibration. These factors will be at the forefront of our investigations to gain deeper insights into their contributions to motor vibrations.

Simultaneously, there have been scarce reports on experimental methods to verify the impact of these individual forces. Therefore, designing well-conceived experiments is crucial and necessary for accurately validating these findings. This aspect is also a part of our future research endeavors. Fortunately, Hong et al. [34] recently addressed this issue. They employed a method involving the wounding windings with a series of unconventional winding structures in a slot and air-gap. By applying a certain regular current to the windings added to the slots, they made it possible to experimentally verify the tangential force-induced vibration of the motor stator. For experimental validation of the radial force-induced vibration of the motor stator, we followed the principles of their approach. We introduced an additional inner stator structure and, by applying a certain regular current to the windings on the inner stator, experimented to verify the isolated effect of the radial force on the motor. Combining both methods allows us to verify the impact of the coupling of these two forces on the vibration characteristics of the motor.

REFERENCES

- [1] A. M. EL-Refaie, "Fractional-slot concentrated-windings synchronous permanent magnet machines: Opportunities and challenges," *IEEE Trans. Ind. Electron.*, vol. 57, no. 1, pp. 107–121, Jan. 2010.
- [2] J. F. Gieras, C. Wang, and J. C. Lai, *Noise of Polyphase Electric Motors*. Boca Raton, FL, USA: CRC Press, 2006.
- [3] F. Magnussen and H. Lendenmann, "Parasitic effects in PM machines with concentrated windings," *IEEE Trans. Ind. Appl.*, vol. 43, no. 5, pp. 1223–1232, Oct. 2007.
- [4] S. Wang, J. Hong, Y. Sun, and H. Cao, "Analysis of zeroth-mode slot frequency vibration of integer slot permanent-magnet synchronous motors," *IEEE Trans. Ind. Electron.*, vol. 67, no. 4, pp. 2954–2964, Apr. 2020.
- [5] H. Fritze, "Noise in electrical machines," in *Archiv für Elektrotechnik*, vol. 10, Berlin, Germany: Springer, 1921, p. 73.
- [6] M. S. Islam, R. Islam, and T. Sebastian, "Noise and vibration characteristics of permanent-magnet synchronous motors using electromagnetic and structural analyses," *IEEE Trans. Ind. Appl.*, vol. 50, no. 5, pp. 3214–3222, Sep. 2014.
- [7] H. Jordan, *Electric Motor Silencer-Formation and Elimination of the Noise in the Electric Motors*. Essen, Germany: W. Girardet, 1950.
- [8] W. Deng and S. Zuo, "Electromagnetic vibration and noise of the permanent-magnet synchronous motors for electric vehicles: An overview," *IEEE Trans. Transport. Electrific.*, vol. 5, no. 1, pp. 59–70, Mar. 2019.
- [9] Y. Lu, J. Li, R. Qu, D. Ye, H. Lu, J. Sun, M. Ge, and H. Xu, "Electromagnetic force and vibration analysis of permanent-magnet-assisted synchronous reluctance machines," *IEEE Trans. Ind. Appl.*, vol. 54, no. 5, pp. 4246–4256, Sep. 2018.
- [10] Y. Lu, J. Li, H. Xu, K. Yang, F. Xiong, R. Qu, and J. Sun, "Comparative study on vibration behaviors of permanent magnet assisted synchronous reluctance machines with different rotor topologies," *IEEE Trans. Ind. Appl.*, vol. 57, no. 2, pp. 1420–1428, Mar. 2021.
- [11] M. Boesing, T. Schoenen, K. A. Kasper, and R. W. De Doncker, "Vibration synthesis for electrical machines based on force response superposition," *IEEE Trans. Magn.*, vol. 46, no. 8, pp. 2986–2989, Aug. 2010.
- [12] H. Yang and Y. Chen, "Influence of radial force harmonics with low mode number on electromagnetic vibration of PMSM," *IEEE Trans. Energy Convers.*, vol. 29, no. 1, pp. 38–45, Mar. 2014.
- [13] S. Hu, S. Zuo, M. Liu, H. Wu, and Z. Liu, "Modeling and analysis of radial electromagnetic force and vibroacoustic behaviour in switched reluctance motors," *Mech. Syst. Signal Process.*, vol. 142, Aug. 2020, Art. no. 106778.
- [14] H. Fang, D. Li, R. Qu, and P. Yan, "Modulation effect of slotted structure on vibration response in electrical machines," *IEEE Trans. Ind. Electron.*, vol. 66, no. 4, pp. 2998–3007, Apr. 2019.
- [15] H. Fang, D. Li, J. Guo, Y. Xu, and R. Qu, "Hybrid model for electromagnetic vibration synthesis of electrical machines considering tooth modulation and tangential effects," *IEEE Trans. Ind. Electron.*, vol. 68, no. 8, pp. 7284–7293, Aug. 2021.
- [16] J.-H. Kim, S.-H. Park, J.-Y. Ryu, and M.-S. Lim, "Comparative study of vibration on 10-pole 12-slot and 14-pole 12-slot PMSM considering tooth modulation effect," *IEEE Trans. Ind. Electron.*, vol. 70, no. 4, pp. 4007–4017, Apr. 2023.
- [17] W. Liang, J. Wang, P. C.-K. Luk, and W. Fei, "Analytical study of stator tooth modulation on electromagnetic radial force in permanent magnet synchronous machines," *IEEE Trans. Ind. Electron.*, vol. 68, no. 12, pp. 11731–11739, Dec. 2021.
- [18] W. Zhao, S. Zhu, J. Ji, G. Liu, and Y. Mao, "Analysis and reduction of electromagnetic vibration in fractional-slot concentrated-windings PM machines," *IEEE Trans. Ind. Electron.*, vol. 69, no. 4, pp. 3357–3367, Apr. 2022.
- [19] H. Yin, H. Zhang, W. Hua, Z. Wu, and C. Li, "Quantitative analysis of electromagnetic forces by decoupling air-gap field modulation and force modulation in rotor-permanent-magnet machines," *IEEE Trans. Ind. Electron.*, vol. 70, no. 2, pp. 1310–1320, Feb. 2023.
- [20] H. Lan, J. Zou, Y. Xu, and M. Liu, "Effect of local tangential force on vibration performance in fractional-slot concentrated winding permanent magnet synchronous machines," *IEEE Trans. Energy Convers.*, vol. 34, no. 2, pp. 1082–1093, Jun. 2019.
- [21] J. F. Hong, L. Gui, and J. C. Cao, "An investigation of tangential force and radial force in PM motor by means of FEM-simulation," in *Proc. Int. Conf. Electr. Mach. (ICEM)*. Valencia, Spain: IEEE, Sep. 2022, pp. 2009–2014.
- [22] Z. Q. Zhu and D. Howe, "Instantaneous magnetic field distribution in brushless permanent magnet DC motors. III. Effect of stator slotting," *IEEE Trans. Magn.*, vol. 29, no. 1, pp. 143–151, Jan. 1993.
- [23] S. Wang, J. Hong, Y. Sun, and H. Cao, "Exciting force and vibration analysis of stator permanent magnet synchronous motors," *IEEE Trans. Magn.*, vol. 54, no. 11, pp. 1–5, Nov. 2018.
- [24] P. L. Timar, A. Fazekas, J. Kiss, A. Miklos, and S. Vang, "Noise and vibration of electrical machines," *Stud. Electr. Electron. Eng.*, vol. 34, Jun. 1989, p. 86.
- [25] V. Mehta and R. Mehta, *Principles of Electrical Machines*. New Delhi, India: S. Chand, 2008, pp. 37–40.
- [26] Z. Xing, X. Wang, and W. Zhao, "Research on weakening measure of radial electromagnetic force waves in permanent magnet synchronous motors by inserting auxiliary slots," *IET Electr. Power Appl.*, vol. 14, no. 8, pp. 1381–1395, Aug. 2020.
- [27] Z. Q. Zhu and D. Howe, "Instantaneous magnetic field distribution in permanent magnet brushless DC motors. IV. Magnetic field on load," *IEEE Trans. Magn.*, vol. 29, no. 1, pp. 152–158, Jan. 1993.
- [28] C.-S. Park, J.-H. Kim, S.-H. Park, and M.-S. Lim, "Effect of electromagnetic force caused by PMSM on the vibration/noise of reciprocating compressors," *IEEE Access*, vol. 11, pp. 56324–56335, 2023.
- [29] Z. Q. Zhu, Z. P. Xia, L. J. Wu, and G. W. Jewell, "Analytical modeling and finite-element computation of radial vibration force in fractional-slot permanent-magnet brushless machines," *IEEE Trans. Ind. Appl.*, vol. 46, no. 5, pp. 1908–1918, Sep. 2010.

- [30] R. Huston and H. Josephs, *Practical Stress Analysis in Engineering Design*. Boca Raton, FL, USA: CRC Press, 2008.
- [31] S. Wu, S. Zuo, X. Wu, F. Lin, H. Zhong, and Y. Zhang, "Vibroacoustic prediction and mechanism analysis of claw pole alternators," *IEEE Trans. Ind. Electron.*, vol. 64, no. 6, pp. 4463–4473, Jun. 2017.
- [32] H. Yin, X. Zhang, F. Ma, C. Gu, H. Gao, and Y. Wang, "New equivalent model and modal analysis of stator core-winding system of permanent magnet motor with concentrated winding," *IEEE Access*, vol. 8, pp. 78140–78150, 2020.
- [33] H. Yin, F. Ma, X. Zhang, C. Gu, H. Gao, and Y. Wang, "Research on equivalent material properties and modal analysis method of stator system of permanent magnet motor with concentrated winding," *IEEE Access*, vol. 7, pp. 64592–64602, 2019.
- [34] J. Hong, L. Gui, and J. Cao, "Analysis and experimental verification of the tangential force effect on electromagnetic vibration of PM motor," *IEEE Trans. Energy Convers.*, vol. 38, no. 3, pp. 1893–1902, Sep. 2023.



XIXIN RAO was born in Jiujiang, China, in 1965. He received the master's degree in engineering from the Nanjing University of Aeronautics and Astronautics, in March 1992, and the Ph.D. degree in mechatronics engineering from Nanchang University, in November 2011.

He is currently a Professor with the School of Mechanical Engineering, Nanchang University. He has presided over and participated in several key research and development projects of the Ministry of Science and Technology, National Natural Science Foundation Projects, and major enterprise cooperation projects. He has published many SCI articles in top international journals. His current research interests include vibration and noise, electronics packaging, and thermal management. His research interests include chip cooling simulation, wind power new energy, and carbon nanotube new material preparation equipment field.



IV RONG is currently pursuing the master's degree with the School of Advanced Manufacturing, Nanchang University, Nanchang, China.

His research interests include the computation of vibration and acoustic noise and the design of permanent magnet machines.



WUSHENG GAN is currently pursuing the master's degree with the School of Advanced Manufacturing, Nanchang University, Nanchang, China.

His research interests include motor vibration and modal analysis.



CHENGDI XIAO received the Ph.D. degree in mechanical engineering from Central South University, Changsha, China, in 2018.

He has been an Associate Professor with Nanchang University, since 2021. He is currently involved in mechanical vibrations and noise thermal management of electronic devices. He has authored over 20 papers. His current research interests include vibration and noise, electronics packaging, and thermal management.



YI ZHOU was a National Household Appliance Standard Committee Refrigeration Equipment Technical Committee Member, a Home Appliance Technology Expert Committee Member, and a Shanghai Electric Group Technology Expert. He is currently the CTO of Shanghai Highly Electric Company Ltd., and a Professor Level Senior Engineer. He has published more than 100 papers and granted more than 70 patents. His current research interest includes research and

development work in the field of home air conditioning compressors.

• • •